NASA TECHNICAL MEMORANDUM

NASA TM X-73664

NASA TM X-73664

(NASA-TM-73664) HOT CORROSION RESISTANCE OF NICKEL-CHROMIUM-ALUMINUM ALLOYS (NASA) 35 p HC A03/MF A01 CSCL 11F

N77-27215

Unclas G3/26 36845

HOT CORROSION RESISTANCE OF NICKEL-CHROMIUM-ALUMINUM ALLOYS

by Gilbert J. Santoro and Charles A. Barrett
Lewis Research Center
Cleveland, Ohio 44135

TECHNICAL PAPER presented at the
One hundred fifty-first Meeting of the Electrochemical Society,
Philadelphia, Pennsylvania, May 8-13, 1977

HOT CORROSION RESISTANCE OF NICKEL-CHROMIUM-ALUMINUM ALLOYS

by Gilbert J. Santoro and Charles A. Barrett
National Aeronautics and Space Administration
Lewis Research Center
Cleveland, Ohio 44135

E-9184

ABSTRACT

The hot corrosion resistance of nickel-chromium-aluminum alloys was examined by cyclically oxidizing sodium sulfate-coated specimens in still air at 900°, 1000°, and 1100° C. The compositions tested were within the ternary region: Ni; Ni-50 at.% Cr; and Ni-50 at.% Al. At each temperature the corrosion data were statistically fitted to a third order regression equation as a function of chromium and aluminum contents. From these equations corrosion isopleths were prepared. Compositional regions with the best hot corrosion resistance were identified.

HOT CORROSION RESISTANCE OF NICKEL-CHROMIUM-ALUMINUM ALLOYS

by Gilbert J. Santoro and Charles A. Barrett
National Aeronautics and Space Administration
Lewis Research Center
Cleveland, Ohio 44135

E-9184

SUMMARY

Alloys in the nickel-chromium-aluminum system were cyclically hot corroded at 900°, 1000°, and 1100° C for 100 hours. The data were statistically treated to obtain corrosion isopleths at each temperature as a function of composition. The results were compared with previous work on the oxidation of these same alloys. Compositions with simultaneously good oxidation and hot corrosion resistance were found to be centered at about Ni-33 at. % Al and Ni-30 at. % Cr-20 at. % Al.

Alloys melted in zirconia crucibles and not annealed have significantly greater hot corrosion resistance at 1100° C than alloys melted in alumina crucibles and annealed. At lower temperatures differences in the preparation of the alloys did not significantly affect their hot corrosion resistance.

INTRODUCTION

In recent years many promising compositions have been identified in the nickel-chromium-aluminum (Ni-Cr-Al) system for use in application requiring a high degree of high-temperature corrosion resistance. Such applications have included coatings for many types of alloys (ref. 1)

and as the matrices for oxide dispersion-strengthened alloys (ref. 2). Recently a program was initiated at NASA-Lewis to determine the optimum compositions with the best balance of cyclic oxidation and hot corrosion resistance, tensile properties, ductility, and strategic element content. In pursuit of this objective an investigation was completed (ref. 3) wherein nickel-rich alloys in the Ni-Cr-Al system were evaluated for their cyclic oxidation resistance in still air at 1100^{o} and 1200^{o} C. A first approximation oxidation attack parameter was derived which was related to the Cr and Al content by a multiple linear regression analysis. The resultant equations were translated into contour diagrams showing regions with minimum oxidation attack. This paper is the 2nd step in the overall program. The same alloys as were used in reference 3, were examined in this study for their hot corrosion resistance by cyclically oxidizing sodium sulfate (Na_2SO_4) coated specimens in still air at 900^{o}, 1000^{o}, and 1100^{o} C. The compositions tested were within the ternary region: Ni; Ni-50Cr and Ni-50Al (all compositions are given in atomic percent in this paper). A limited number of alloys were coated with Na_2SO_4 containing 10 weight percent sodium chloride (NaCl) in order to determine the effect of NaCl on the corrosion process. The extent of the corrosion was determined by the specimen's net weight change, the maximum depth of attack, and by the weight of its spalls. The maximum depth of attack data, being the least ambiguous measure of the corrosion, were related to Cr and Al content at each temperature by a multiple linear regression analysis. The resultant third order regression equations were translated into

corrosion isopleths which indicated compositional regions of minimum attack. The corrosion contours from this study were compared to those from reference 3 for oxidation resistance and regions of simultaneously good oxidation and hot corrosion resistance were identified.

MATERIALS

All of the alloys specifically prepared for this program were vacuum melted in zirconia (ZrO_2) crucibles and cast in zirconia shell molds. The zirconium (Zr) pickup of up to 0.6 weight percent was detected. Each mold consisted of a tree of ten 2.5- by 5.1- by 0.25- centimeter coupons, each with its own riser. For each coupon used the risers were removed and analyzed by atomic absorption for chromium and aluminum. The composition of these alloys are given in table I, casting 1-11.

Most of the supplement alloys used in this study were obtained from a previous program (ref. 4) and had been melted in alumina (Al_2O_3) crucibles and cast into 1.9 cm diameter cyclindrical ZrO_2 molds. These castings had been annealed 24 hours at 1200^{o} C in quartz tubes which had been evacuated and backfilled with argon and sealed. Their compositions are given in table I, castings 15-27. Another supplemental alloy was arc-melted in a copper mold (casting 13 of table I). Finally the commerical alloy, IN-671, was also tested as its composition is essentially Ni-50.9Cr, see table I.

All the specimens used in this investigation were glass-bead blasted, ultrasonically cleaned in alcohol, and weighed prior to testing.

Metallographic examination of the as-cast materials revealed four general types of structures. Figure 1(a) is a single-phase structure

typical of γ-nickel solid solution, of γ' (Ni_3Al), and of β (NiAl). Figure 1(b) shows the γ, γ' structure found in most nickel-base superalloys. Figure 1(c) represents the γ', β structure and finally figure 1(d) consists of a blocky structure of γ' and β with small particles of chromium solid solution (αCr) in the β. Table I lists the as-cast phases of the alloys tested in this study and figure 2 is a phase diagram of the region of interest (ref. 5).

PROCEDURES

Test Procedures

Prior to testing sample dimensions were measured and in particular the thickness was measured to a precision of ±1 micrometer. Prior to exposure in the furnace, samples were coated with 1 mg/cm^2 of Na_2SO_4, or in some cases 1 mg/cm^2 of the mixture Na_2SO_4 + 10 weight percent NaCl. Application of the salt coating was accomplished by heating a weighed sample on a hot plate set at about 200^o C and spraying one side with a saturated solution of salt using an airbrush. The sample was then cooled and weighed to check for the correct amount of salt deposition. The same procedure was used to coat the other side of the specimen. The samples were then ready for the cyclic specimen furnace which has been described in detail in reference 6. Samples were thermally cycled to allow one hour at temperature and a minimum of 40 minutes cooling in static air. A typical temperature profile is shown in figure 3. Samples reached the highest test temperature in less than 2 minutes after insertion into the furnace and cooled to ambient temperature in less than 20 minutes after removal from the furnace. Samples of each alloy were exposed for 100 cycles at 900^o, 1000^o, and 1100^o C.

Weight change was determined at regular intervals throughout the test. At the conclusion of the furnace testing the accumulated spall for each sample was weighed and examined by x-ray diffraction. Each corroded sample was also examined by x-ray diffraction and by metallography. The thickness of the alloy visibly unaffected by the corrosion attack was measured on metallographically prepared cross-sections with a microscope cathetometer at a magnification of 100X. The original thickness minus the above measurement all divided by two then is defined here as the maximum depth of penetration of the corrosion attack.

Statistical Procedures

A digital computer program, NEWRAP, reference 7 was used to perform the regression analyses. A two independent variable polynomial model was apriori judged as suitable for this data. The dependent variable was the maximum depth of corrosion, D, and the two independent variables were C and A, the atomic percent concentrations of chromium and aluminum respectively in the alloy. The approach was to begin with a first order polynomial and to go to higher order equations if necessary. The decision as to which order polynomial provided the best fit was judged from the fraction of total variation (total sum of squares) accounted for by a particular regression equation and how reasonable were the predictions of this equation at locations away from the data points. This fraction of the total variation explained by the regression equation is called the coefficient of determination, R^2.

Nonsignificant terms were deleted from the model by the back-rejection technique where the critical significance level is supplied

as input. The strategy used here for a given order equation was to minimize the standard error of estimate and still predict reasonable values over the composition range.

It is possible to significantly increase the R^2 of a regression equation by including other factors that might account for a significant added fraction of the variabiiity. This is accomplished by the addition of a dummy variable, Z, and setting it either to 0 or 1. Thus in reference 3 the alloys were divided into two groups - those melted in zirconia crucibles and not annealed, Z = 1, and those that were melted in alumina crucibles and annealed, Z = 0. The addition of the dummy variable significantly raised the R^2 and lowered the standard error of estimate. From this result it was inferred that zirconia impurity affected the oxidation resistance. The dummy variable approach was included in this study for each of the three temperature regression runs.

In corrosion studies of this type the dependent variable (in this case the maximum depth of attack, D) usually has the same relative error over a wide range of values. This situation requires the dependent variable to be transformed to the logarithm of the variable. The process is termed homogenizing the error variance.

RESULTS

Measure of Corrosion

The extent of corrosion was measured by the net specific weight change, the accumulated weight of spall and the maximum depth of attack. In general all three measures gave consistent results. Samples which changed little in weight usually spalled only slightly and had relatively little depth of attack. The reverse statement is also generally

true. Figure 4(a) to (c), contains the weight change data from 900° to 1100° C of a random selection of the alloys tested. The values in parenthesis following the alloy designations are the maximum depth of attack in micrometers and the values in brackets are the specific accumulated spall weight in milligrams per centimeter squared. The data can be classified into three categories:

(1) Alloys with relatively little weight change.

(2) Alloys with substantial weight gains.

(3) Alloys with substantial weight losses.

A complete set of the corrosion data is presented in tabular form in table II where the temperature dependence for each alloy is readily discernable. Thus at 900° C only alloy 17 spalled (and then but slightly) while many samples spalled at 1100° C. Comparing the last two columns of table II, specific net weight change and specific weight of accumulated spall, a negative weight change in the former column ought to be accompanied by a nearly equal weight of spall in the latter column. A fair comparison is observed in this respect for most of the alloys with the notable exception of alloys 22 and 23. For these two alloys there is a large net weight loss but no detectable spall. Since a spall shield surrounded the specimens when they were cooling, a large fraction of the spall should have been collected even if the specimens spalled exposively. Thus it must be assumed these two specimens had spalled either at temperature or while being raised out of the furnace.

X-ray Diffraction And Metallography

After the furnace exposure both the retained and the spalled oxides were identified by x-ray diffraction. These oxide phases are listed in

table III. With but few exceptions all specimens formed multi-oxide phases. Figure 5(a) to (c), is a graphical presentation of the x-ray diffraction data. For the purpose of this figure the spalled and retained oxide data were combined. The figure illustrates two major points. The presence of chromium in the alloy decreases the aluminum content needed for Al_2O_3 formation in the scale. An explanation of this result is given reference 8. The other point is that with increased temperature more aluminum is required in the alloy for Al_2O_3 formation. The opposite behavior occurs in straight oxidation because of the increased diffusivity of the aluminum ion with temperature. But under the hot corrosion conditions of this study the spalling increased with temperature and overshadowed this effect. Thus at higher temperatures a greater aluminum content in an alloy is necessary to maintain a sufficient level to compensate for that lost due to the increased spalling.

The modes of attack during hot corrosion are described in table III by listing three major morphological aspects frequently observed in corroded alloys and by identifying which ones are applicable to each of the alloys tested. The three modes are: (1) oxide penetration, often along grain boundaries; (2) formation of a depleted zone immediately beneath the scale; and (3) internal corrosion products and/or void formation. Examples of these corrosion modes are presented in figure 6(a) and (b).

Sodium Chloride Effect

Table IV summarizes the data concerning the effect of adding NaCl to the Na_2SO_4 on the hot corrosion of a limited number of alloys. At 900^{o} C the effect is quite apparent. The NaCl caused the scale to spall

and thereby accelerated the attack. Also NiO was a prominent phase in the spall of all specimens indicating a depletion in their surface concentration of aluminum and chromium. This result agrees with literature reports indicating sodium chloride vapors can disrupt the protective scale of alloys, reference 9 and 10.

At 1100° C the effect of the NaCl is not so evident. NiO was consistently a predominent phase of the spall of specimens with NaCl in their coating but was not always detected in the spalls of specimens corroded in the absence of NaCl. However at 1100° C the presence of NaCl did not seem to be consistently detrimental to the corrosion resistance of the alloys.

DISCUSSION

How a material corrodes depends not only upon its composition but also upon the testing parameters used. Since there are many hot corrosion testing procedures in use today (ref. 11) it would be very difficult to directly compare the corrosion results obtained here with those of other laboratories. Of course the ultimate test procedure would be to test the material in actual application, e.g. in a gas turbine engine. This procedure is not practical for use with all candidate materials and a number of screening type tests are required so that only a few "best" candidates are chosen for the actual application test. The procedure used in this investigation must be considered as a screening type test. Its value lies in the identification of those "best" compositions for further testing.

Based upon the data collected in this study, a mutiple linear regression analysis was used to identify the "best" compositions in the

Ni-rich end of the Ni-Cr-Al system. The procedure used was discussed earlier. The maximum depth of attack data, being the least ambiguous measure of the corrosion, were chosen to relate corrosion to the Cr and Al content of the alloys at each temperature. A summary of the statistical data appears in table V(a) to (c), and is called the analysis of variance table (ANOVA). Included are the final regression equations. The third order, two independent variables regression equations were translated by a computer program into corrosion isopleths. Figure 7(a) to (c), are the resultant contours at 900^{o}, 1000^{o}, and 1100^{o} C respectively. Although the contours are related to the logarithm of the maximum depth of attack in micrometers, log D, the values listed in figure 7 within the contours are D directly. At 900^{o} C a large minimum attack area exists at the higher chromium, higher aluminum compositions. At 1000^{o} C this area decreases in size. At 1100^{o} C two small areas of minimum attack exists at the edges of the diagram, one centered at about Ni-30Cr-20Al and the other centered at Ni-33Al. These two areas overlap areas of minimum oxidation attack observed in reference 3 and shown here in figure 8.

One effect of increasing temperature is to increase the rate of corrosion which in turn provides a better separation of the corrosion resistance of the alloys. But a surprising feature of figure 7 is that alloys with very low aluminum content corroded more at 1000^{o} C than they did at 1100^{o} C. Since the vapor pressure of Na_2SO_4 at 1100^{o} C is moderate, 10^{-1} Nm^{-2} (10^{-6} atm.) reference 12, the decrease in corrosion at 1100^{o} C for these low aluminum containing alloys cannot be attributed entirely to

the loss of Na_2SO_4 via vaporization.* The entire Na_2SO_4 coating can be lost, however, by the spalling of the outer portion of the scale. Having lost their Na_2SO_4 coatings the alloys could then heal themselves and further corrosion would be by pure oxidation and at a much lower rate. Figure 7(c) then could represent the recovery ability of those hot corroded alloys that spalled. And most of the alloys at 1100° C did spall. Since the best hot corrosion resistant compositions in figure 7(c) overlap the best oxidation resistant compositions in figure 8, it can be generalized that for these alloys the ones with the best oxidation resistance have the best hot corrosion recovery ability. In gas turbines the exposure to hot corrosion conditions is thought to be intermittent (ref. 10). Thus the ability of material to recover from an hot corrosion attack could be an important factor in the life of that material when used in gas turbine engines.

As was done in reference 3 a dummy variable was used to determine if a significant variation could be ascribed to differences in the preparation of the alloys. One set of alloys came from a previous program (ref. 4) and were melted in Al_2O_3 crucibles and annealed. The alloys

---

* Fred J. Kohl (NASA-Lewis) extrapolated his 900° C rate data from slowly flowing oxygen and calculated a rate of vaporization of 3.5×10^{-2} mg/cm^2 hr.$^{-1}$ for 1100° C. This value would represent an upper limit as the tests in this paper were conducted in still air. Thus sodium sulfate (or perhaps more correctly its reacted products) ought to be present throughout most of the 100 hours duration of these tests.

prepared specifically for this program were melted in zirconia crucibles and were not annealed. No significant preparation effect could be detected for the 900° C data, i.e., there was not a significant rise in R^2 or lowering of the standard error of estimate. Only a small effect could be detected for the 1000° C data. But at 1100° C a marked difference was detected. The statistical data and the regression equations are listed in table V(d). Figure 9(a) and (b) are the resultant corrosion isopleths. Figure 9(a), where the dummy variable was set to zero, applies to alloys melted in Al_2O_3 crucibles and annealed. Figure 9(b), where the dummy variable was set to one, applies to alloys melted in ZrO_2 crucibles and not annealed. Analogous to the oxidation of these alloys (ref. 3) the latter preparation of the alloys provided superior corrosion resistance. Thus either trace amounts of ZrO_2 and/or the absence of annealing has a significant beneficial effect on the hot corrosion resistance of Ni-Cr-Al alloys.

SUMMARY OF RESULTS

Alloys in the nickel-chromium-aluminum system were cyclically hot corroded at 900°, 1000°, and 1100° C for 100 hours. The data were statistically treated to obtain corrosion isopleths at each temperature as a function composition. The hot corrosion results were compared with previous work on the oxidation of these same alloys. The results of this work are summarized as follows:

1. Compositions with simultaneously good oxidation and hot corrosion resistance were found to be centered at about Ni-33Al and Ni-30Cr-20Al.

2. Alloys melted in zirconia crucibles and not annealed had significantly greater hot corrosion resistance at 1100° C than alloys melted in alumina crucibles and annealed. At lower temperatures differences in the preparation of the alloys did not significantly affect their hot corrosion resistance.

3. At low temperatures, the presence of NaCl in the Na_2SO_4 caused the scales of the samples to spall and thereby to increase their rate of corrosion.

REFERENCES

1. E. J. Felten, T. E. Strangman, and N. E. Ulion, PWA-5091, Pratt and Whitney Aircraft, East Hartford, Conn. (1974); also NASA CR-134735.
2. D. H. Timbres, L. F. Norris, and M. A. Glegg, Sherritt Gordon Mines, Ltd. (AD-748266; AFML-TR-72-50), Fort Saskatchewan, Alberta (1972).
3. C. A. Barrett and C. E. Lowell, NASA Tech Note D-8255 (1976).
4. G. J. Santoro, D. L. Deadmore, and C. E. Lowell, NASA Tech Note D-6414 (1971).
5. A. Taylor and R. A. Floyd, J. Inst. Met., 81, 451 (1952-1953).
6. C. A. Barrett and C. E. Lowell, Oxid. Met., 9, 307 (1975).
7. S. M. Sidik, NASA Tech Note D-6770 (1972).
8. R. Kosak, Jr., Ph. D. Thesis, Ohio State Univ., Columbus (1969).
9. P. Hancock, in "Proceedings of 1974 Gas Turbine Materials in the Marine Environment Conference," MCIC-75-27, J. W. Fairbanks and I. Machlin, Editors, p. 225, Metals and Ceramics Information Center, Battelle Columbus Labs., Oh. (1975).

10. J. F. G. Conde and B. A. Wareham, in "Proceedings of 1974 Gas Turbine Materials in the Marine Environment Conference," MCIC-75-27, J. W. Fairbanks and I. Machlin, Editors, p. 73, Metals and Ceramics Information Center, Battelle Columbus Labs., Oh. (1975).

11. J. Stringer, MCIC-72-08, Metals and Ceramics Information Center (AD-745474), Battelle Columbus Labs., Oh., (1972).

12. F. J. Kohl, C. A. Stearns, and G. C. Fryburg, in "Metal-Slag-Gas Reactions and Processes," Z. A. Foroulis and W. W. Smeltzer, Editors, p. 649, The Electrochem. Soc., Inc., Princeton, N. J. (1975).

TABLE I. - CHEMISTRY AND PHASES OF THE ALLOYS

Alloys	Composition at. %		As cast phases
	Cr	Al	
1	15.98	17.54	γ', β
2a	11.50	25.58	γ', β, α
2b	12.44	22.72	γ', β, α
3	13.19	12.07	γ, γ'
4	18.42	11.06	γ, γ'
5a	14.35	23.65	γ', β, α
5b	16.89	29.19	γ', β, α
6a	19.15	24.16	γ', β, α
6b	19.19	24.24	γ', β, α
7	15.81	5.77	γ
8a	18.87	26.99	γ', β, α
8b	20.84	16.52	γ', β, α
9	9.73	17.18	γ, γ'
10	19.87	-	γ
11	38.70	-	γ
a_{13}	-	41.78	β
b_{15}	0.78	24.50	γ'
b_{16}	2.86	22.60	γ'
b_{17}	9.96	15.73	β
b_{20}	2.60	47.60	β
b_{21}	10.30	39.10	β
b_{22}	2.80	7.10	γ
b_{23}	1.20	8.90	γ
b_{27}	Remelted and cast nickel-200 (99.6%)		γ
c_{IN-671}	50.90	(.39Ti-.23C)	γ, α

(a) Arc melted ingots in copper molds.
(b) Melted in Al_2O_3 crucibles and annealed.
(c) Commerical alloy, nominal composition.

TABLE II. - CYCLIC HOT CORROSION OF NICKEL-CHROMIUM-ALUMINUM ALLOYS

[Specimens coated with 1mg/cm^2 of sodium sulfate (Na_2SO_4); 100 hours at temperature.]

Alloy	Temperature °C	Maximum depth of attack, μM	Specific weight change, mg/cm^2	Specific weight of accumulated spall, mg/cm^2
1	900	3	0	0
	1000	22	-2	2
	1100	140	-7	10
2a	900	2	0	0
	1000	35	0	1
	1100	68	-14	5
2b	1000	0	-1	0
	1100	168	-14	13
3	900	30	4	0
	1000	96	-33	38
	1100	254	-61	73
4	900	22	0	0
	1000	82	-16	17
	1100	362	-18	25
5a	900	0	0	0
	1000	19	-2	1
	1100	85	-10	5
5b	900	0	0	0
	1000	0	0	0
	1100	90	-6	0
6a	900	0	0	0
	1000	15	-4	2

TABLE II. - continued

Alloy	Temperature °C	Maximum depth of attack, μM	Specific weight change, mg/cm^2	Specific weight of accumulated spall, mg/cm^2
6b	900	0	0	0
	1000	0	0	0
	1100	163	-6	4
7	900	99	4	0
	1000	102	-4	6
	1100	291	-15	18
8a	900	0	0	0
	1000	20	0	0
	1100	84	-2	2
8b	900	6	0	0
	1000	4	-2	0
	1100	231	-7	7
9	900	18	0	0
	1000	138	-35	49
	1100	187	-58	70
10	900	54	0	0
	1100	155	-106	107
11	1100	113	-3	3
13	900	20	29	0
	1000	52	10	7
	1100	164	1	2

TABLE II. - continued

Alloy	Temperature °C	Maximum depth of attack, μM	Specific weight change, mg/cm^2	Specific weight of accumulated spall, mg/cm^2
15	900	50	4	0
	1000	54	6	0
	1100	153	-59	66
16	900	67	7	0
	1000	162	16	1
	1100	272	-138	-
17	900	14	4	1
	1000	131	-47	52
	1100	299	-111	123
20	900	2	1	0
	1000	125	9	0
	1100	-	114	1
20	900	-	1	0
	1000	156	4	0
	1100	-	97	1
21	900	0	0	0
	1000	208	12	0
	1100	-	34	2
21	900	0	0	0
	1000	156	7	0
	1100	515	24	0
22	900	87	6	0
	1000	233	23	7
	1100	709	-515	0

Table II. - continued

Alloy	Temperature °C	Maximum depth of attack, μM	Specific weight change, mg/cm^2	Specific weight of accumulated spall, mg/cm^2
23	900	94	6	0
	1000	150	20	0
	1100	373	-267	0
27 (Ni-200)	900	55	18	0
	1000	-	11	4
	1100	205	20	3
IN-671	900	68	2	0
	1000	98	-1	1
	1100	139	1	1

TABLE III. - OXIDE PHASES AND MODE OF MICROSTRUCTURAL ATTACK

Alloy	Temp. °C	Oxide Phases*		Mode of Attack		
		Retained scale	Spalled scale	Oxide penetration	Depleted zone	Internal corrosion or voids
1	900	spinel, Cr_2O_3, Al_2O_3	no spall detected	no	no	no
	1000	Cr_2O_3	Al_2O_3, spinel, Cr_2O_3	no	yes	no
	1100	Cr_2O_3, spinel	NiO, Al_2O_3, spinel	no	yes	yes
2a	900	Cr_2O_3, Al_2O_3	no spall detected	no	no	no
	1000	------	NiO, spinel	no	yes	no
	1100	Al_2O_3, Cr_2O_3	spinel, Al_2O_3	no	yes	no
2b	1000	spinel, Al_2O_3, Cr_2O_3(?)	spinel, Al_2O_3	no	no	no
	1100	Al_2O_3, spinel, Cr_2O_3	spinel, Al_2O_3	no	yes	yes
3	900	NiO, Al_2O_3, Cr_2O_3	no spalls detected	no	yes	no
	1000	NiO	NiO, spinel	no	yes	no
	1100	NiO, spinel	NiO, spinel	yes	yes	yes
4	900	Al_2O_3, Cr_2O_3	no spalls detected	no	yes	no
	1000	Cr_2O_3	NiO, spinel	yes	yes	yes
	1100	spinel, Cr_2O_3	NiO, spinel, Cr_2O_3	yes	yes	yes
5a	900	Cr_2O_3, Al_2O_3	no spalls detected	no	no	no
	1000	------	Al_2O_3, spinel	no	yes	no
	1100	Al_2O_3, spinel	Al_2O_3, spinel	no	yes	yes
5b	900	Al_2O_3	no spalls detected	no	no	no
	1000	Al_2O_3, spinel	no spalls detected	no	no	no
	1100	Al_2O_3, spinel	Al_2O_3, spinel, Cr_2O_3	yes	yes	no
6a	900	Al_2O_3	no spalls detected	no	no	no
	1000	------	Al_2O_3, spinel	no	slight	no

* Listed in order of decreasing line intensities. (?) Insufficient lines for positive identification.

TABLE III. - continued

Alloy	Temp. °C	Oxide Phases*		Mode of Attack		
		Retained scale	Spalled scale	Oxide penetration	Depleted zone	Internal corrosion or voids
7	900	NiO, Cr_2O_3, Al_2O_3, spinel	NiO, spinel	yes	no	no
	1000	NiO, spinel	NiO, spinel	yes	no	yes
	1100	NiO, spinel, Cr_2O_3	NiO, spinel, Cr_2O_3	yes	no	yes
8a	900	Al_2O_3	no spalls detected	no	no	no
	1000	Al_2O_3	no spalls detected	no	yes	no
	1100	Al_2O_3, spinel, Cr_2O_3	Al_2O_3, NiO	yes	yes	yes
8b	900	Al_2O_3	no spalls detected	no	no	no
	1000	Al_2O_3, Cr_2O_3	spinel, Al_2O_3	no	no	no
	1100	Cr_2O_3, Al_2O_3, spinel	spinel, NiO, Al_2O_3, Cr_2O_3	no	yes	yes
9	900	Al_2O_3, spinel	no spalls detected	no	slight	no
	1000	NiO, spinel, Al_2O_3, Cr_2O_3	NiO, Cr_2O_3	no	yes	no
	1100	Al_2O_3, Cr_2O_3	NiO, spinel	some	yes	yes
10	900	NiO, spinel	no spalls detected	no	no	yes
	1100	NiO, spinel, Cr_2O_3	NiO, spinel, Cr_2O_3	no	no	yes
11	1100	Cr_2O_3, spinel	Cr_2O_3	no	no	yes
13	900	NiO, Al_2O_3	no spalls detected	no	no	no
	1000	Al_2O_3, NiO	NiO, Al_2O_3, spinel	yes	yes	no
	1100	NiO, Al_2O_3, spinel	NiO, Al_2O_3, spinel	yes	yes	no
15	900	NiO, Al_2O_3, spinel	NiO, Al_2O_3	no	no	no
	1000	NiO, spinel, Al_2O_3	NiO, Al_2O_3, spinel	no	slight	no
	1100	NiO, spinel, Al_2O_3	NiO, Al_2O_3	yes	yes	no

* Listed in order of decreasing line intensities.

TABLE III. - continued

Alloy	Temp. °C	Oxide Phases*		Mode of Attack		
		Retained scale	Spalled scale	Oxide penetration	Depleted zone	Internal corrosion or voids
16	900	NiO, spinel, Al_2O_3	NiO	no	no	no
	1000	NiO, spinel, Al_2O_3	NiO	no	no	no
	1100	NiO, spinel, Al_2O_3	NiO, Al_2O_3	yes	yes	yes
17	900	NiO, spinel	NiO	no	yes	no
	1000	NiO, spinel, Al_2O_3, Cr_2O_3	NiO	no	yes	yes
	1100	NiO, Spinel, Al_2O_3, Cr_2O_3	NiO	yes	yes	yes
20	900	Al_2O_3	no spalls detected	no	no	no
	1000	Al_2O_3	NiO, Al_2O_3, spinel	some	yes	no
	1100	Al_2O_3, spinel	NiO, spinel(?)	yes	yes	no
21	900	Al_2O_3	no spalls detected	no	no	no
	1000	Al_2O_3, spinel	no spalls detected	yes	yes	no
	1100	Al_2O_3, Cr_2O_3, spinel	Al_2O_3, NiO	yes	yes	no
22	900	NiO	no spalls detected	no	no	no
	1000	NiO	NiO	no	no	no
	1100	NiO	NiO, spinel	no	no	no
23	900	NiO	no spalls detected	no	no	no
	1000	NiO	no spalls detected	no	no	no
	1100	NiO, spinel(?)	NiO, spinel	no	no	no

* Listed in order of decreasing line intensities. (?) Insufficient lines for positive identification.

TABLE III. - continued

Alloy	Temp., °C	Oxide Phases*		Mode of Attack		
		Retained scale	Spalled scale	Oxide penetration	Depleted zone	Internal corrosion or voids
27 (Ni-200)	900	NiO	No spalls detected	no	no	no
	1000	NiO	NiO	no	no	no
	1100	NiO	NiO	no	no	no
IN-671	900	Cr_2O_3	No spalls detected	no	yes	yes
	1000	Cr_2O_3	Cr_2O_3	no	yes	yes
	1100	Cr_2O_3, spinel(?)	Cr_2O_3	no	yes	yes

* Listed in order of decreasing line intensities. (?) Insufficient lines for positive identification.

TABLE IV. - EFFECT OF SODIUM CHLORIDE (NaCl) ON THE CORROSION ATTACK

A. Amount of Corrosion

Alloy	900°C						1100°C					
	Na_2SO_4			Na_2SO_4 + 10 w/o NaCl			Na_2SO_4			Na_2SO_4 + 10 w/o NaCl		
	MDA[a]	S[b]	ΔW[c]	MDA	S	ΔW	MDA	S	ΔW	MDA	S	ΔW
1	3	0	0	19	2	-2	140	10	-7	232	36	-31
2a	2	0	0	21	<1	0	68	5	-14	46	18	-21
3	30	0	4	28	2	8	254	73	-61	295	59	-49
4	22	0	0	29	10	-2	362	25	-18	326	37	-27
5a	0	0	0	9	<1	-1	85	5	-10	65	9	-18
9	18	0	0	16	<1	3	187	70	-58	247	87	-73

(a) MDA Maximum depth of attack, μM.

(b) S Specific weight of accumulated spall, mg/cm^2

(c) ΔW Specific weight change, mg/cm^2.

TABLE IV. - continued

B. Oxide Phases in the Scale*- 900°C

Alloy	Na_2SO_4		Na_2SO_4 + 10 w/o NaCl	
	Retained Scale	Spalled Scale	Retained Scale	Spalled Scale
1	spinel, Cr_2O_3, Al_2O_3	none detected	spinel, Al_2O_3, Cr_2O_3, NiO	NiO, spinel, Cr_2O_3
2a	Cr_2O_3, Al_2O_3	none detected	Al_2O_3, spinel, NiO, Cr_2O_3(?)	NiO, spinel
3	NiO, Al_2O_3, Cr_2O_3	none detected	NiO, spinel, Al_2O_3, Cr_2O_3	NiO, spinel Cr_2O_3(?)
4	Al_2O_3, Cr_2O_3	none detected	NiO, spinel, Cr_2O_3, Al_2O_3	NiO, spinel
5a	Cr_2O_3, Al_2O_3	none detected	NiO, spinel, Al_2O_3	NiO, spinel
9	Al_2O_3, spinel	none detected	NiO, spinel, Al_2O_3	NiO, spinel

* Listed in order of decreasing line intensities.

(?) Insufficient lines for positive identification.

TABLE IV. - continued

C. Oxide Phases in the Scale* - 1100°C

Alloy	Na_2SO_4		Na_2SO_4 + 10 w/o NaCl	
	Retained Scale	Spalled Scale	Retained Scale	Spalled Scale
1	Cr_2O_3, spinel	NiO, Al_2O_3, spinel	spinel, NiO, Cr_2O_3, Al_2O_3	NiO, spinel
2a	Al_2O_3, Cr_2O_3	spinel, Cr_2O_3	NiO, spinel, Al_2O_3, Cr_2O_3	NiO, spinel
3	NiO, spinel	NiO, spinel	spinel, NiO, Al_2O_3, Cr_2O_3	NiO, spinel
4	spinel, Cr_2O_3	NiO, spinel, Cr_2O_3	spinel, NiO, Cr_2O_3, Al_2O_3	NiO, spinel
5a	Al_2O_3, spinel	Al_2O_3, spinel	spinel, Al_2O_3, NiO, Cr_2O_3	NiO, Cr_2O_3, spinel
9	Al_2O_3, Cr_2O_3	NiO, spinel	NiO, spinel, Al_2O_3, Cr_2O_3	NiO, spinel

* Listed in order of decreasing line intensities.

(?) Insufficient lines for positive identification.

TABLE V. - ANALYSIS OF VARIANCE

A. Data at 900°C

Source	Sums of squares	Degrees of freedom	Mean squares	Calculated F value
Regression	31.126461	4	7.7816153	78.80((compared to $F(4,19,0.95) \approx 5.81$))
Residual	1.876195	19	.0987471	
Total	33.002656	23		

R^2 = SSQ(REG)/SSQ(TOT) = .943150

Standard error of estimate = .314241

$$\log D = 1.81689 + 9.11839\times10^{-2}A - 5.26785\times10^{-3}A^2 - 5.65473\times10^{-3}CA + 6.45260\times10^{-5}A^3$$

D = maximum depth of corrosion, uM
C = at. % chromium
A = at. % aluminum

TABLE V. - continued

B. Data at 1000°C

Source	Sums of squares	Degrees of freedom	Mean squares	Calculated F value
Regression	2.087594	5	.4175188	9.97((compared to $F(5,14,0.95) \approx 4.63$))
Residual	.586315	14	.0418796	
Total	2.673909	19		

R^2 = SSQ(REG)/SSQ(TOT) = .780727

Standard error of estimate = .204645

$$\log D = 2.20239 + 8.18814\times10^{-2}C - 1.69504\times10^{-3}C^2 - 2.10706\times10^{-4}A^2 - 9.28978\times10^{-3}CA + 2.18724\times10^{-4}CA^2$$

D = maximum depth of corrosion, uM

C = at. % chromium

A = at. % aluminum

TABLE V. - continued

C. Data at 1100°C

Source	Sums of squares	Degrees of freedom	Mean squares	Calculated F value
Regression	1.097560	5	.2195120	10.09((compared to $F(5,17,0.95) \approx 4.59$))
Residual	.369896	17	.0217586	
Total	1.467456	22		

R^2 = SSQ(REG)/SSQ(TOT) = .747934

Standard error of estimate = .147508

$$\log D = 2.17186 + .143390A - 9.52439\times10^{-3}A^2 - 3.05352\times10^{-3}CA + 1.47265\times10^{-4}A^3 + 1.14503\times10^{-4}CA^2$$

D = maximum depth of corrosion, uM

C = at. % chromium

A = at. % aluminum

TABLE V. - continued

D. Data at 1100°C with dummy variable

Source	Sums of squares	Degrees of freedom	Mean squares	Calculated F value
Regression	1.230196	8	.1537745	9.07((compared to $F(8,14,0.95) \simeq 3.23$))
Residual	.237260	14	.0169471	
Total	1.467456	22		

R^2 = SSQ(REG)/SSQ(TOT) = .838319

Standard error of estimate = .130181

$$\log D = 2.29753 + 2.41902\times10^{-2}C + 0.101384A - 5.34642\times10^{-4}C^2 - 7.20886\times10^{-3}A^2$$
$$- 1.42786\times10^{-3}CA + 1.14005\times10^{-4}A^3 + 6.04861\times10^{-5}CA^2 - 0.363850Z$$

D = maximum depth of corrosion, uM
C = at. % chromium
A = at. % aluminum
Z = dummy variable: Z = 0, melted in Al_2O_3 crucible and annealed.
Z = 1, melted in ZrO_2 crucible and not annealed.

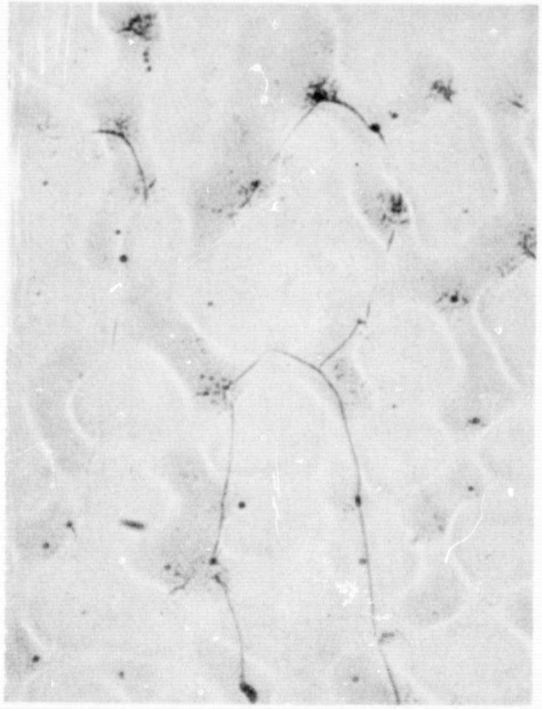

(a) Ni-15.81 Cr-5.77 Al; γ phase.

(b) Ni-973 Cr-17.18 Al; γ + γ' phase.

Figure 1. Representative microstructures in the Ni-Cr-Al system.

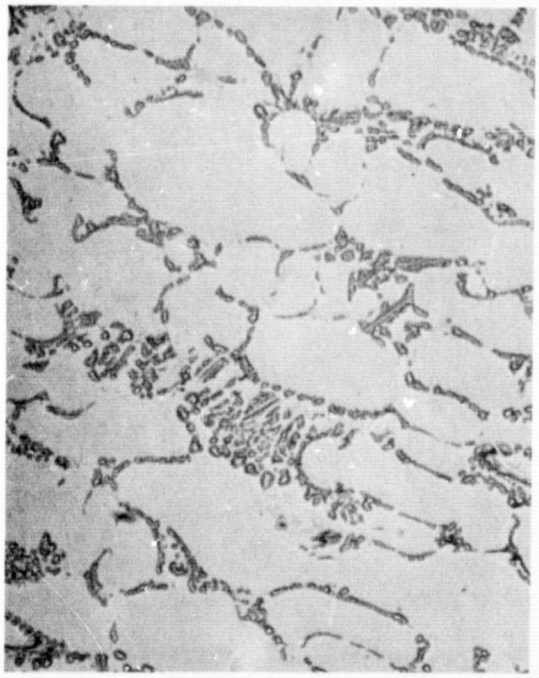

(c) Ni-15.98 Cr-17.54 Al; γ' + β phase.

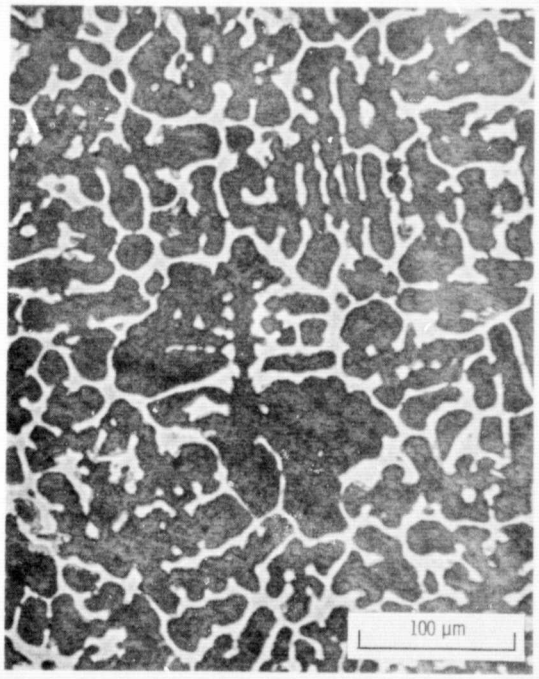

(d) Ni-11.5 Cr-25.58 Al; γ' + β + α phase.

Figure 1. - Concluded.

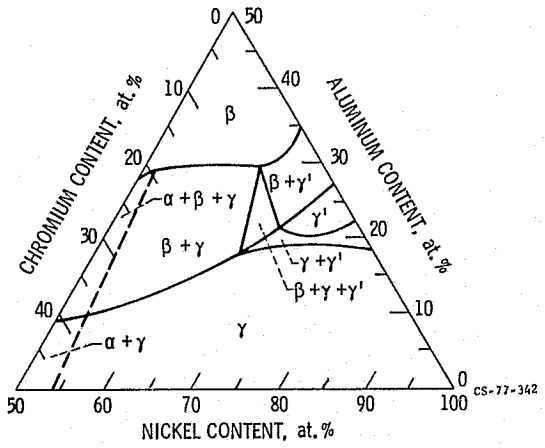

Figure 2. - Phase diagram in the Ni-Cr-Al system at 1100° C after Taylor and Floyd (ref. 5).

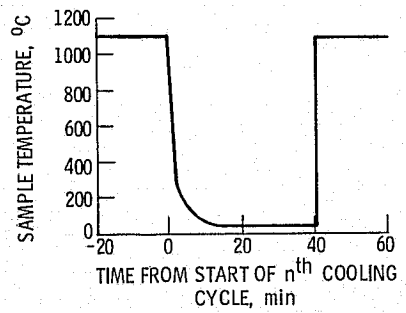

Figure 3. - Temperature profile of typical thermal cycle.

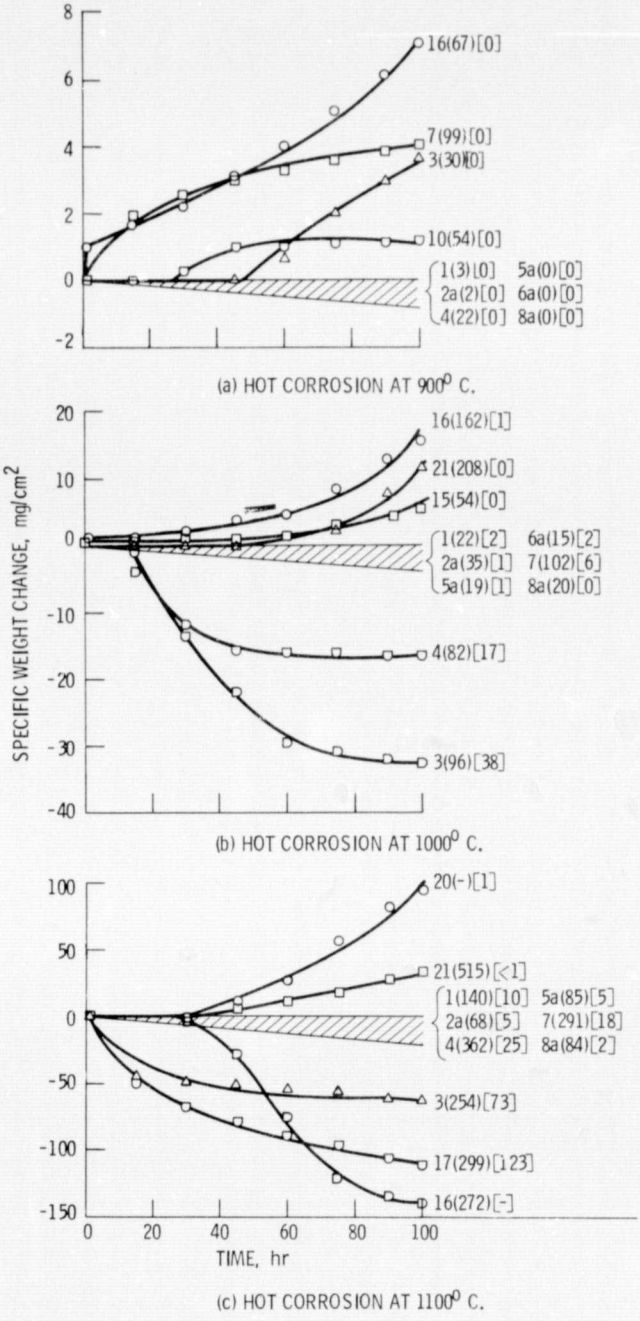

Figure 4. - The first number designates the alloy; the number in parenthesis is the maximum depth of attack, μm; the number in brackets is the specific accumulated spall weight, mg/cm^2.

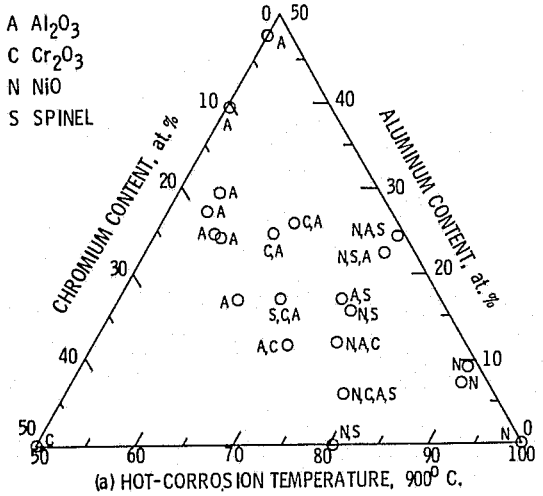

(a) HOT-CORROSION TEMPERATURE, 900° C.

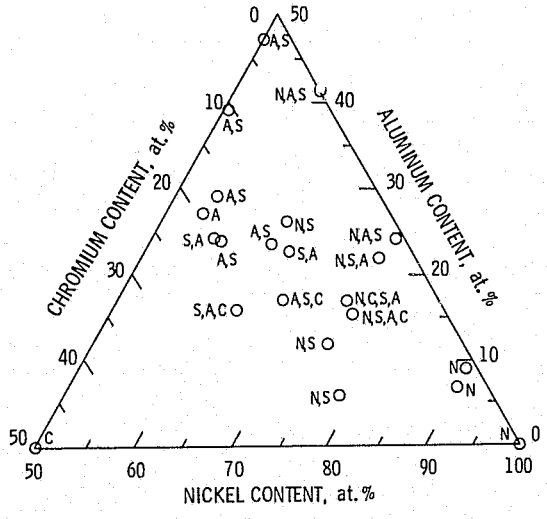

(b) HOT-CORROSION TEMPERATURE, 1000° C.

Figure 5. - Oxide phases in the scale of hot-corroded specimens. (Phases are listed in order of decreasing line intensities.)

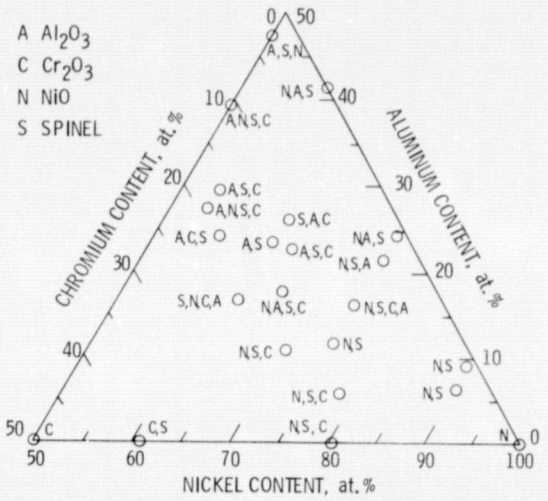

(c) HOT-CORROSION TEMPERATURE, 1100° C.

Figure 5. - Concluded.

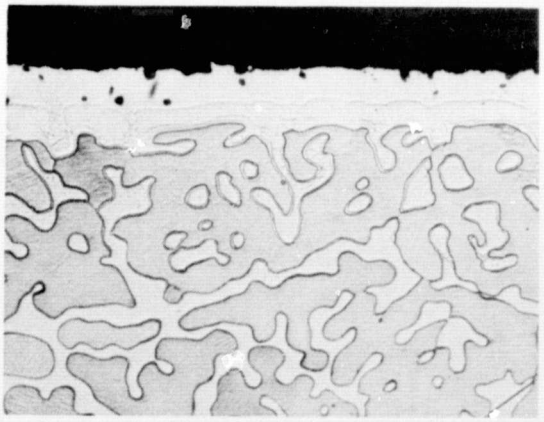

(a) A $\gamma' + \beta + \alpha$ alloy, Ni-11.50 Cr-25.58 Al shows a thin retained scale, a depleted zone, and the unaffected alloy.

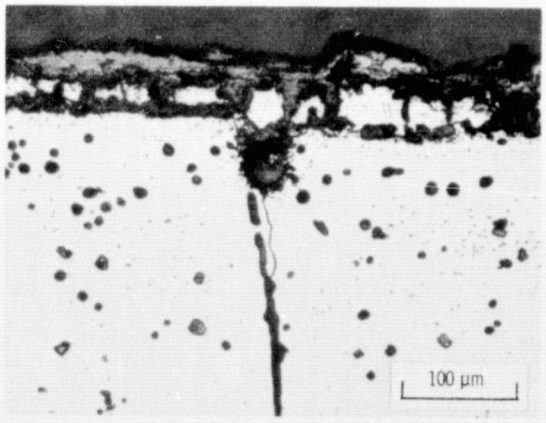

(b) A γ alloy, Ni-15.81 Cr-5.77 Al shows a thick retained scale, oxide penetration and internal corrosion extending deep into the alloy.

Figure 6. - Hot corroded Ni-Cr-Al alloys at 1100° C showing typical corrosion morphologies.

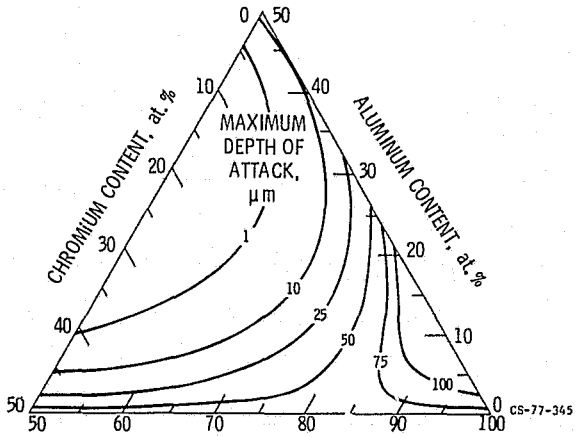

(a) AT 900° C. (EQUATION FOR CONTOURS GIVEN IN TABLE V(a).)

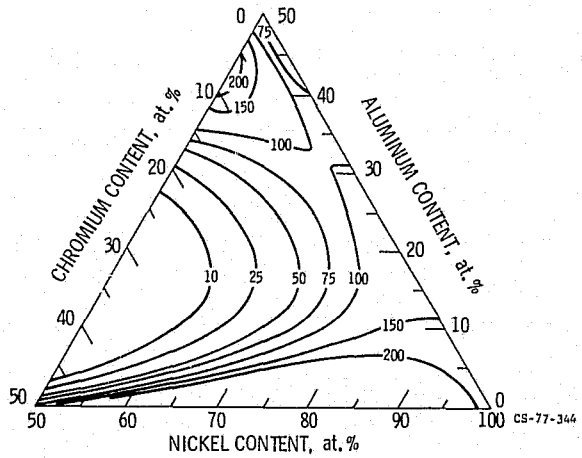

(b) AT 1000° C. (EQUATION FOR CONTOURS GIVEN IN TABLE V(b).)

Figure 7. - Hot corrosion isopleths.

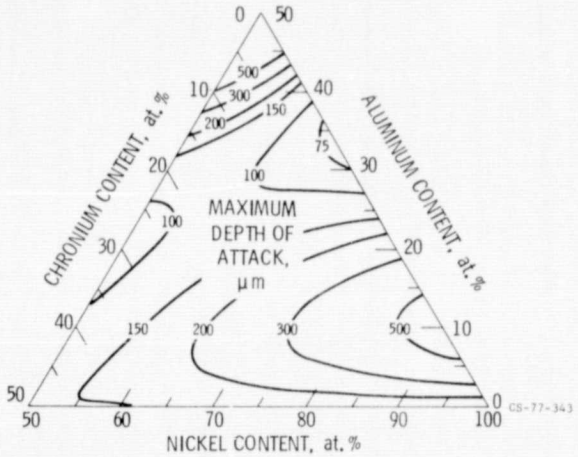

(c) AT 1100° C. (EQUATION FOR CONTOURS GIVEN IN TABLE V(c).)

Figure 7. - Concluded.

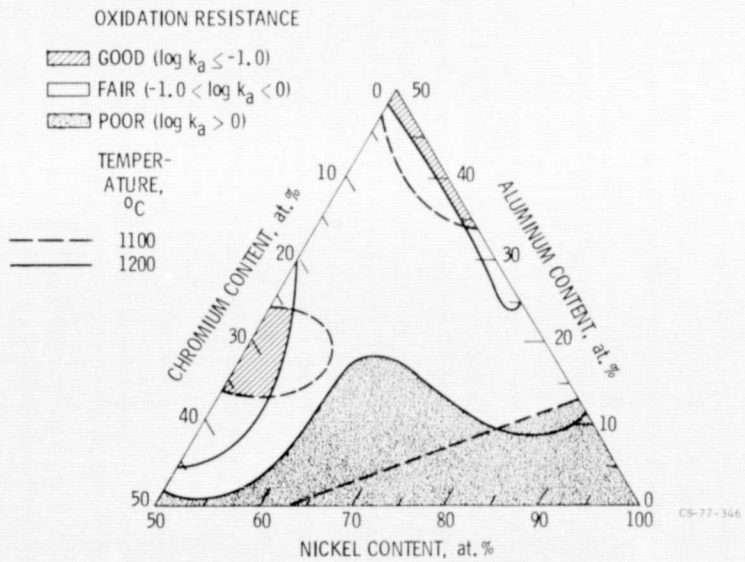

Figure 8. - Overall cyclic oxidation resistance for Ni-Cr-Al alloys at 1100° and 1200° C in still air; reference 3.

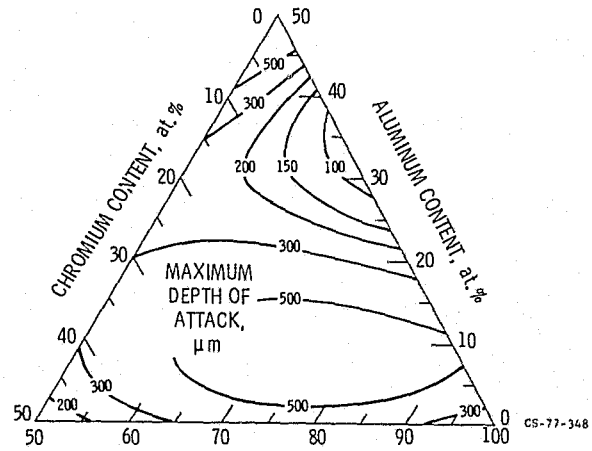

(a) INCORPORATING DUMMY VARIABLES Z = 0.

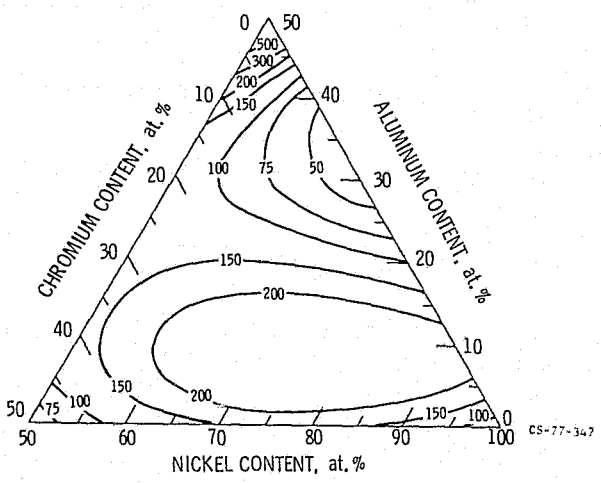

(b) INCORPORATING DUMMY VARIABLE Z = 1.

Figure 9. - Hot corrosion isopleths at 1100° C. (Equation for contours given in table V(d).)